Available online at www.sciencedirect.com
ScienceDirect
Journal of the European Ceramic Society 30 (2010) 2265–2277
www.elsevier.com/locate/jeurceramsoc

Near net-shape/net-dimension ZrC/W-based composites with complex geometries via rapid prototyping and Displacive Compensation of Porosity

David W. Lipke [a], Yunshu Zhang [a], Yajun Liu [a,1], Benjamin C. Church [a,2], Kenneth H. Sandhage [a,b,*]

[a] School of Materials Science and Engineering, Georgia Institute of Technology, Atlanta, GA 30332, USA
[b] School of Chemistry and Biochemistry, Georgia Institute of Technology, Atlanta, GA 30332, USA

Available online 9 February 2010

Abstract

ZrC/W-based composites with complex shapes have been fabricated by combining rapid prototyping methods for synthesizing porous WC preforms with the shape/dimension-preserving, reactive infiltration-based Displacive Compensation of Porosity (DCP) process. Two automated rapid prototyping methods were examined: (i) computer-numerical-controlled machining of porous WC powder compacts, and (ii) 3D printing of WC powder. After binder removal and partial sintering (to neck the WC particles), the shaped, porous, and rigid preforms were exposed to molten Zr_2Cu at 1150–1300 °C and ambient pressure. Upon infiltration, the Zr in the melt underwent a displacement reaction with WC to yield more voluminous ZrC and W products that filled prior pores (reaction-induced densification). The resulting ZrC/W-based composites retained the shapes and dimensions (to within 1%) of the WC preforms. This work demonstrates, for the first time, that rapid preform prototyping can be integrated with the DCP process to generate dense, ultrahigh-melting carbide/refractory metal composites with tailorable near net-shapes and -dimensions.

Keywords: Carbides; Composites; Shaping; Wear Parts; Displacive Compensation of Porosity

1. Introduction

Advances in the performance of aerospace vehicles have been, and are likely to continue to be, strongly linked to the development of advanced materials. Among the most extreme environments experienced by aerospace materials is generated within solid-fueled rocket nozzles. The combustion of solid, aluminum-bearing fuels results in rapid heating to temperatures in excess of 2500 °C and yields molten aluminum oxide and gas products traveling at supersonic speeds.[1–8] Refractory rocket nozzle materials need to be highly resistant to thermal shock and to recession by erosion, vaporization, or thermochemical spallation.[2–8] Composites comprised of carbides and refractory metals can possess attractive combinations of properties for such extreme environments. Consider, for example, composites of zirconium carbide and tungsten. Zirconium carbide is a hard (up to 28.4 GPa), high-melting (up to 3445 °C) compound that is much lighter than tungsten (i.e., the densities of ZrC and W are 6.63 g/cm^3 and 19.26 g/cm^3, respectively).[9–11] Tungsten is also quite high-melting (3422 °C) but undergoes a brittle-to-ductile transformation at ≤360 °C.[12–15] Hence, composites of ZrC and W should possess higher stiffness and reduced weight relative to monolithic tungsten, and higher resistance to fracture at elevated temperatures relative to monolithic zirconium carbide. Song et al. have reported that hot pressed W/ZrC composites with 30 vol% ZrC have exhibited higher values of elastic modulus than monolithic W from room temperature to 1200 °C (with values of about 345 GPa for W/ZrC vs. about 270 GPa for W at 1200 °C) and fracture strengths in 3-point bending up to 810 MPa at 1200 °C.[16] Zirconium carbide and tungsten are also chemically and thermally compatible. ZrC and W possess low vapor pressures and exhibit limited mutual solid solubility at elevated temperature and ambient pressure.[17,18] Furthermore, these solids do not react to form other more stable compounds at ambient pressure.[17] ZrC and W possess similar thermal expansion coefficients at room temperature (4.0×10^{-6}/°C for ZrC and 4.5×10^{-6}/°C for W) and at 2700 °C (10.2×10^{-6}/°C for

* Corresponding author at: School of Materials Science and Engineering, Georgia Institute of Technology, 771 Ferst Drive, Atlanta, GA 30332, USA. Tel.: +1 404 894 6882.
E-mail address: ken.sandhage@mse.gatech.edu (K.H. Sandhage).
[1] Present address: Western Transportation Institute, Montana State University, Bozeman, MT 59715, USA.
[2] Present address: Materials Department, University of Wisconsin-Milwaukee, Milwaukee, WI 53201, USA.

0955-2219/$ – see front matter © 2010 Elsevier Ltd. All rights reserved.
doi:10.1016/j.jeurceramsoc.2010.01.011

ZrC and 9.2×10^{-6}/°C for W).[19,20] Both materials also possess relatively high values of thermal conductivity (40 ± 10 W/m K for ZrC and 105 ± 10 W/m K for W over the temperature range of 1000–2200 °C).[21,22] Such a combination of mechanical, chemical, and thermal properties makes ZrC/W composites attractive for applications involving highly erosive environments at elevated temperatures,[23] such as for solid Al-fueled rocket nozzles.

While W/ZrC composites have been prepared by hot pressing of powder mixtures (e.g., using an applied stress of 20 MPa at 2000 °C for 1 h), this approach is not well-suited for fabricating complex-shaped composites such as rocket nozzles.[16] Zhang et al. have recently reported a solid-state reaction sintering approach for preparing W/ZrC composites comprised of 35 vol% to 50 vol% ZrC with relative densities of 94.5% to >98%, respectively.[24] Dickerson et al. have used a reactive infiltration process to convert porous WC preforms into 96.5–99.6% dense ZrC/W-based composites containing 50–60 vol% ZrC with little change (<1%) in dimensions and shape.[25,26] This patented process, known as the Displacive Compensation of Porosity, involves the use of volume-increasing liquid/solid displacement reactions to fill the pores within rigid, shaped ceramic-bearing preforms.[27–32] The reactive (pressureless) infiltration of Zr_2Cu(l) into rigid, porous WC preforms at 1150–1300 °C resulted in the formation of ZrC/W-based composites via the following displacement reaction:

$$0.5Zr_2Cu(l) + WC(s) = ZrC(s) + W(s) + 0.5Cu(l) \quad (1)$$

The replacement of WC with the more voluminous ZrC and W products caused the pores within the rigid preforms to become filled with these latter solids (i.e., reaction-induced densification), thereby forcing Cu-rich liquid product out of the composite. Because the solid ZrC and W products possess a combined volume that is 2.01 times the WC volume, the WC within preforms with ≥50.2 vol% porosity could be completely consumed to yield co-continuous ZrC/W-based composites that retained the starting preform shape and dimensions.[11] Small amounts of residual copper trapped within the dense composites could be utilized as a transpirational cooling agent at elevated temperatures (*note*: copper does not react with zirconium carbide or tungsten to form new compounds and exhibits negligible solid solubility in tungsten).[33] By tailoring the phase content (i.e., through the use of controlled amounts of WC, W_2C, W, and/or ZrC) and porosity of the starting preform, ZrC/W-based composites with a range of ZrC and W contents have been synthesized.[34–37]

DCP-derived ZrC/W-based rocket nozzle liners, fabricated by reactive infiltration of a porous, nozzle-shaped WC preform prepared by gel casting, have been found to be resistant to the extreme thermal shock and erosion conditions of a solid-fueled Pi–K rocket test.[25] While gel casting is an effective and scalable method for fabricating complex-shaped 3D WC preforms, this casting process required the fabrication of a multipart mold with the an internal geometry appropriate for a particular nozzle configuration. The use of mold-free rapid prototyping methods for fabricating WC preforms would allow for rapid variations in preform geometries that, in turn, could be rapidly converted into dense, near net-shape/net-dimension ZrC/W-based composites for subsequent component testing (e.g., rocket tests of nozzle and nozzle liners with varied configurations). While rapid prototyping methods have been used to prepare porous preforms for other reactive infiltration processes, no work has been conducted to date on the integration of rapid prototyping methods with a reactive infiltration process capable of generating dense, near net-dimension, ultrahigh-melting (>2500 °C) ceramic/metal composites.[38–42] The purpose of this paper is to evaluate the use of two rapid prototyping methods, 3D printing and computer-numerical-controlled (CNC) machining, for fabricating shaped, porous WC preforms for subsequent conversion into dense, near net-shape/net-dimension ZrC/W-based composites.

2. Experimental procedures

Porous, rigid WC preforms with nozzle, cone, crucible, and disk shapes were prepared by: (i) computer-numerical-controlled (CNC) machining of partially sintered WC powder compacts or by (ii) partial sintering of 3D printed WC green bodies. For both approaches, the starting WC powder (obtained from Advanced Materials Technologies, Morristown, TN or Global Tungsten and Powders Corp., Towanda, PA) possessed a purity of 99.9% and an average diameter of 5–6 μm.

2.1. Computer-numerical-controlled machining of porous tungsten carbide preforms

WC/binder mixtures were prepared by blending WC powder with 2.5 wt% of an aqueous solution of 70 wt% ammonium acetate (Sigma–Aldrich, Inc., St. Louis, MO). The mixture was allowed to dry in an evacuated desiccator containing a calcium sulfate desiccant (W.A. Hammond DRIERITE Co. Ltd., Xenia, OH). To further refine and uniformly distribute the ammonium acetate binder, the WC/binder mixture was ball milled with WC media (99% purity, 9.5 mm diameter, Salem Specialty Ball Company, Inc., Canton, CT) within a 7 cm diameter polyethylene jar rotating at 260 rpm for 4 h. The WC/binder mixture was then formed into 5.7 cm diameter cylinders with thicknesses of 1.0 cm or 3.5 cm (for subsequent CNC machining of disk-shaped or nozzle-shaped preforms, respectively) via uniaxial pressing at a peak pressure of 1.7 MPa. Removal of the ammonium acetate binder was conducted by heating in flowing argon (99.999% purity, Airgas, Atlanta, GA) scrubbed of oxygen (Model OG-120 Gas Purification Furnace, Oxy-Gon Industries, Epsom, NH) at a rate of 0.5 °C/min to 160 °C and then holding at this temperature for 4 h. The preforms were then thermally treated at 1450 °C for 4 h in the flowing, oxygen-scrubbed argon to allow for necking of the WC particles within the preforms. The latter heat treatment was conducted to enhance green strength for CNC machining and to avoid specimen shape distortion due to capillary pressures upon subsequent reactive infiltration.

Green bodies were also prepared with the use of starch as a binder. WC powder was mixed with 2.5 wt% rice starch (Catalogue No. 102955, MP Biomedicals, LLC, Solon, OH) using a paint shaker (Red Devil 5400, Red Devil Equipment Co., Ply-

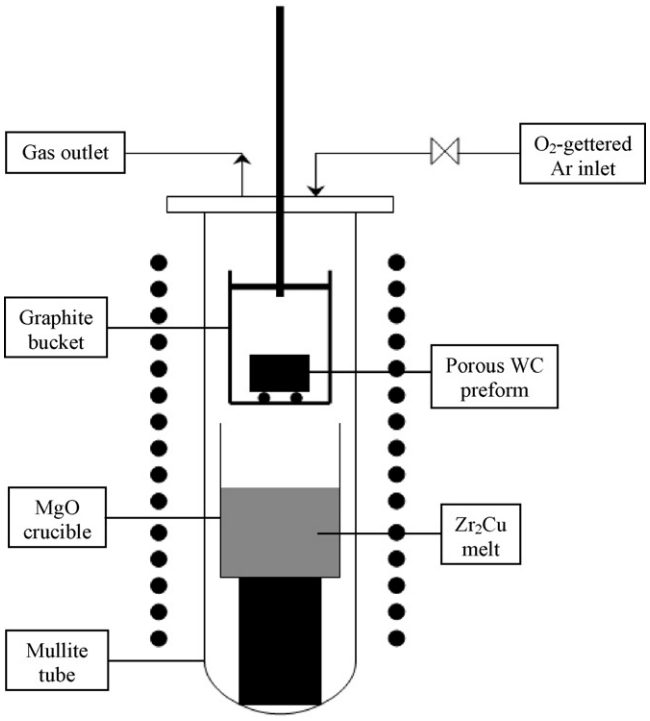

Fig. 1. Schematic of the controlled-atmosphere infiltration apparatus.

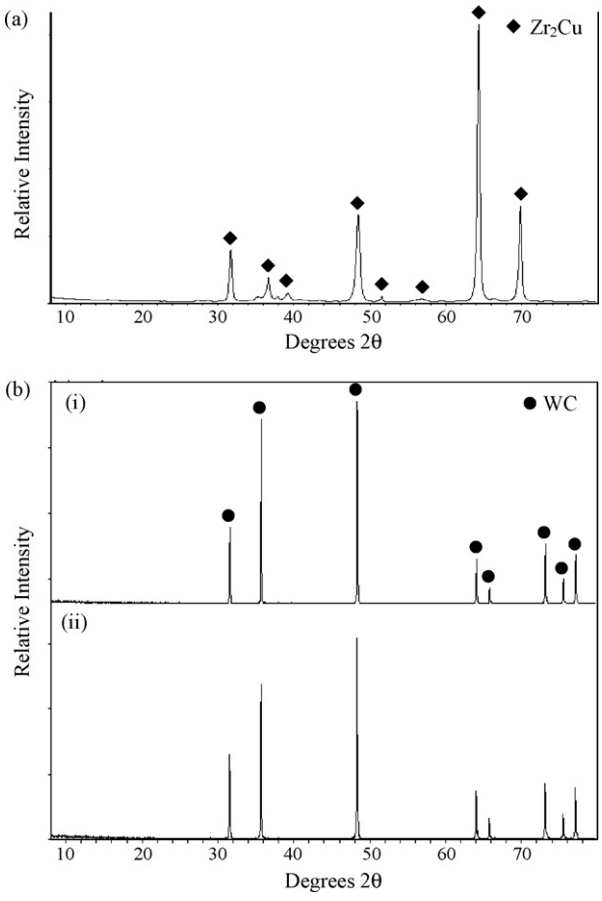

Fig. 2. X-ray diffraction analyses of: (a) a Zr_2Cu ingot (i.e., the melt precursor) prepared by arc melting, (b) porous disk-shaped WC preforms generated by: (i) uniaxial pressing of a WC/rice starch mixture, binder burnout, and partial sintering (for WC particle necking) at 1450 °C for 4 h, and (ii) 3D printing of WC, powder, binder burnout, and partial sintering (for WC particle necking) at a peak temperature of 2100 °C for 4 h.

mouth, MN) for 20 min. The WC/starch mixture was uniaxially pressed into 5.7 cm diameter cylinders with a thickness of 3.5 cm at a peak stress of 35 MPa. The shaped WC preforms were then heated in flowing oxygen-scrubbed argon at a rate of 0.5 °C/min to 275 °C and held at this temperature for 6 h. The preforms were then heated in the oxygen-scrubbed argon at a rate of 2 °C/min to 1000 °C, at which point the flowing argon was replaced with a flowing mixture of CO/CO_2 (9:1 volume ratio) that was maintained for 12 h at 1000 °C. The shaped, binder-free preforms were then thermally treated at 1450 °C for 4 h in oxygen-gettered argon to allow for necking of the WC particles.

These rigid WC preforms possessed bulk densities of 7.56 ± 0.31 g/cm^3, which corresponded to relative densities of $48.3 \pm 2.0\%$ (porosity values of $51.7 \pm 2.0\%$). Machining of such rigid, porous WC compacts was conducted with a CNC milling machine (Model 7300 Prototyping and Production Mill, Flashcut CNC, Deerfield, IL) using a 3.2–6.4 mm diameter WC/Co milling bit. The target shapes (nozzles, surface-patterned disks, cones, crucibles) and dimensions for the machined preforms were entered directly into a CAD software package (SolidWorks 2007, Dassault Systèmes Solidworks Corp., Concord, MA) interfaced with software (DeskProto Version 4.1, Delft Spline Systems, Utrecht, The Netherlands) for conversion into machine tool paths for operation of the milling machine.

2.2. Three-dimensional printing of porous tungsten carbide preforms

WC preforms were prepared in a layer-by-layer fashion with a computer-controlled 3D printer (ZPrinter 310, Z Corp., Burlington, MA). Each layer deposition was conducted by using a roller to spread a ~0.1 mm thick layer of WC powder followed by applying a binder solution through a jet printhead in a desired pattern. The binder solution consisted of 2.5 wt% polyethyleneimine (PEI, branched, MW 10,000) and 0.25 wt% glycerol (both obtained from Polysciences Inc., Warrington, PA) dissolved in de-ionized water. The shape and dimensions of desired preforms were entered directly into a CAD software package interfaced with the printer. Upon completion of printing, the WC preforms were heated to 150 °C for 1 h to cure the binder. After removing excess loose powder with an air brush, the binder in the shaped WC preforms was removed by heating in flowing oxygen-scrubbed argon at a rate of 5 °C/min to 400 °C and then holding at this temperature for 2 h. The WC preforms were then thermally treated at 1400 °C for 2 h in oxygen-scrubbed argon to allow for necking of the WC particles to provide sufficient green strength for preform handling. The preform was then further thermally treated at 2100 °C for 4 h in the oxygen-scrubbed argon within a graphite element furnace (Model TC300, Oxy-gon Industries) to allow for additional necking of the WC particles (i.e., to survive capillary

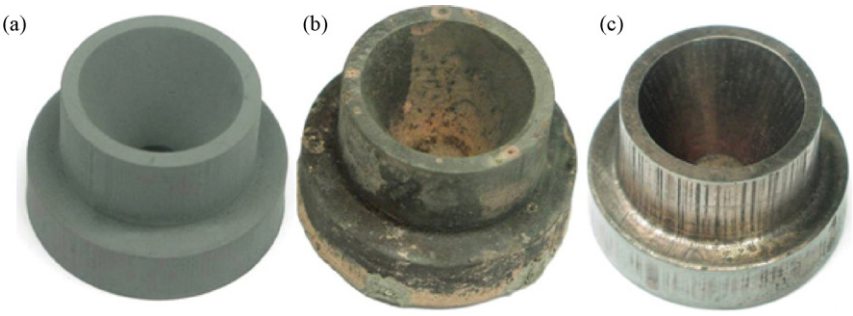

(d)

Specimen Description	Outer Diameter at Nozzle Exit	Outer Diameter at Nozzle Entrance	Nozzle Height
Porous (50.0%) CNC-machined WC preform (before infiltration)	50.65 ± 0.09 mm	37.50 ± 0.08 mm	32.13 ± 0.22 mm
ZrC/W-bearing nozzle (after reactive infiltration)	50.32 ± 0.16 mm	37.23 ± 0.07 mm	32.00 ± 0.30 mm
	$100{\cdot}\Delta D/D_o$(ave.) = -0.65%	$100{\cdot}\Delta D/D_o$(ave.) = -0.72%	$100{\cdot}\Delta L/L_o$(ave.) = -0.40%

Fig. 3. Optical photographs of three rocket nozzle-shaped samples at various stages of fabrication. (a) A porous, rigid WC preform prepared by uniaxial pressing of a WC/binder (ammonium acetate) mixture, binder burnout, partial sintering (for necking of WC particles) at 1450 °C for 4 h, and then CNC machining. (b) and (c) ZrC/W-bearing nozzle-shaped specimens prepared by immersion of CNC-machined, porous WC preforms in the Zr_2Cu melt at 1150 °C for 30 min, then further reaction above the melt at 1300 °C for 2 h. The residual adherent Cu-rich metal present on the specimen surfaces in (b) was removed from the specimen shown in (c). (d) Measured dimensions of the reactively-infiltrated nozzle in (c), and of the associated porous preform prior to infiltration.

pressures generated during subsequent reactive infiltration). After the 2100 °C/4 h treatment, these rigid WC preforms possessed bulk densities of 6.60 ± 0.03 g/cm^3, which corresponded to relative densities of $42.1 \pm 0.2\%$ (porosities of $57.9 \pm 0.2\%$).

2.3. Preparation of the zirconium–copper alloy

Congruently-melting Zr_2Cu ingots were prepared by arc melting. Zr ingots (99.9% purity, 5 cm diameter × 1.5 cm thick, Zirconium Research Corp., Philomath, OR) and Cu rods

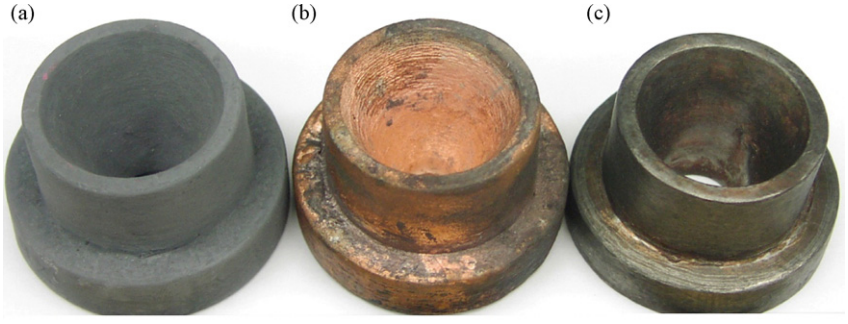

(d)

Specimen Description	Outer Diameter at Nozzle Exit	Outer Diameter at Nozzle Entrance	Nozzle Height
Porous (58.0%) 3-D printed WC preform (before infiltration)	54.23 ± 0.25 mm	40.34 ± 0.20 mm	34.82 ± 0.15 mm
ZrC/W-bearing nozzle (after reactive infiltration)	53.90 ± 0.12 mm	40.09 ± 0.13 mm	34.53 ± 0.23 mm
	$100{\cdot}\Delta D/D_o$(ave.) = -0.61%	$100{\cdot}\Delta D/D_o$(ave.) = -0.62%	$100{\cdot}\Delta L/L_o$(ave.) = -0.83%

Fig. 4. Optical photographs of 3D printed, rocket nozzle-shaped specimens at various stages of fabrication. (a) A porous, rigid WC preform prepared by 3D printing followed by binder burnout and partial sintering (for necking of WC particles) at 1400 °C for 2 h and then 2100 °C for 4 h. (b) and (c) ZrC/W-bearing nozzle-shaped specimens prepared by immersion of 3D printed, porous WC preforms in the Zr_2Cu melt at 1150 °C for 30 min, then further reaction above the melt at 1300 °C for 2 h. The residual adherent Cu-rich metal present on the specimen surfaces in (b) was removed from the specimen shown in (c). (d) Measured dimensions of the reactively-infiltrated nozzle in (c), and of the associated porous preform prior to infiltration.

(a) (b)

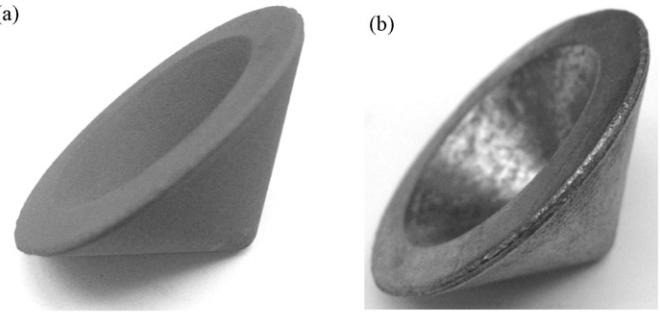

(c)

Specimen Description	Largest Outer Diameter of Cone	Cone Height
Porous (51.5%) 3-D CNC-machined WC preform (before infiltration)	52.40 ± 0.08 mm	26.03 ± 0.05 mm
ZrC/W-bearing specimen (after reactive infiltration)	51.98 ± 0.15 mm	25.87 ± 0.07 mm
	$100 \cdot \Delta D/D_o$(ave.) = -0.80%	$100 \cdot \Delta L/L_o$(ave.) = -0.61%

Fig. 5. Optical photographs of a cone-shaped sample at various stages of fabrication. (a) A porous, rigid, cone-shaped WC preform prepared by uniaxial pressing of a WC/binder (ammonium acetate) mixture, binder removal and partial sintering (for necking of WC particles) at 1450 °C for 4 h, and then CNC machining. (b) A ZrC/W-bearing cone-shaped specimen prepared by immersion of the CNC-machined, porous, cone-shaped WC preform in (a) in the Zr_2Cu melt at 1150 °C for 30 min, then further reaction above the melt at 1300 °C for 2 h, and removal of residual adherent Cu-rich metal from the external surfaces. (c) Measured dimensions of the reactively-infiltrated specimen in (b), and of the associated porous preform in (a) prior to infiltration.

(2.5 cm × 1.5 cm × 0.95 cm) cut from a bar (99.9% purity, McMaster-Carr, Atlanta, GA) were placed on a water-cooled hearth within the evacuable chamber of an arc melting apparatus (Model 5BJ, Centorr Vacuum Industries, Nashua, NH). Prior to arc melting, the chamber was evacuated and backfilled with high-purity argon (scrubbed of oxygen as described above) three times. After first melting a sacrificial piece of zirconium with the arc (to allow for additional gettering of oxygen within the sealed chamber), the arc was used to melt the Zr and Cu pieces and to stir the resulting disk-shaped Zr–Cu melt for several minutes. After solidification, the ingot disc was flipped while within the argon atmosphere chamber of the arc melter, and the disc was then remelted. Such solidification, flipping, and remelting was conducted five times (for a total of six melting steps) to allow for chemical homogenization. The disk-shaped ingots were then broken into pieces of several cm in size for use in generating the Zr_2Cu bath for immersion and reactive infiltration of the porous WC preforms.

2.4. Pressureless reactive infiltration (Displacive Compensation of Porosity)

Reactive infiltration of porous WC preforms by the Zr_2Cu melt was conducted in a high-purity, oxygen-scrubbed argon atmosphere within a vertical tube furnace, as illustrated in Fig. 1. A given porous WC preform was placed inside a graphite bucket (6.4 cm internal dia. × 12.7 cm internal height, >99.9% purity, GraphiteStore.com, Inc., Buffalo Grove, IL) into which several 1 cm dia. holes had been drilled to allow for inflow of molten Zr_2Cu. The preform-containing bucket was positioned above a MgO crucible (12 cm internal dia. × 20 cm internal height, 99.4% purity, Ozark Technical Ceramics, Webb City, MO) containing the Zr_2Cu ingot pieces. Prior to reactive infiltration, the furnace tube was evacuated and backfilled three times with high-purity, oxygen-scrubbed argon. The furnace was then heated to 1150 °C and held at this temperature for 1 h to melt the Zr_2Cu, and to allow for thermal equilibration of the melt and WC preform within the graphite bucket. The graphite bucket was then lowered into the melt to allow the Zr_2Cu(l) to migrate through holes in the bucket and then to completely immerse the WC preform. After 30 minutes of immersion, the graphite bucket was raised out of the melt to allow excess molten metal to drain from the infiltrated preform. The furnace was then heated to 1300 °C and held at this temperature for 2 h to allow for further reaction of the infiltrated melt with residual WC within the specimen. After cooling to room temperature within the oxygen-gettered argon atmosphere, the specimen was removed from the furnace.

2.5. Materials characterization

To allow for evaluation of preform bulk densities, the volumes of internal cavities within the 3D preforms were obtained by pressing modeling compound (Hasbro, Pawtucket, RI) into the preform cavities, and then measuring the volume of such modeling compound via fluid displacement. Archimedes measurements, using water as the buoyant fluid, were used to obtain bulk density values for reactively-infiltrated specimens. Specimen dimensions were measured with a digital caliper (Model CD-6 CSX, Mitutoyo Corp., Kawasaki, Japan). Reactively-infiltrated specimens were cross-sectioned by electrodischarge machining (Charmilles 290P, GF AgieCharmilles LLC, Lincolnshire, IL). Such cross-sections were mounted in epoxy and then ground and polished with a series of diamond pastes to a surface finish of 1 μm. Microstructural analyses of these polished cross-sections were conducted with a field emission gun scanning electron microscope (Leo 1530 FEG SEM, Carl Zeiss SMT Ltd., Cambridge, UK) equipped with an energy dispersive X-ray spectrometer (INCA EDS, Oxford Instruments, Bucks, UK).

X-ray diffraction (XRD) analyses of the phase content of the starting Zr_2Cu ingots, of WC preforms, and of reactively-infiltrated specimens were conducted with Cu Kα radiation at a scan rate of 3°/min (X-Pert ProAlpha 1 diffractometer, PANalytical, Almelo, The Netherlands). To allow for quantification of phase content, XRD calibration curves were generated from mixtures of W (Type C80, 99.8% purity, >40 μm ave. diameter, Buffalo Tungsten, Inc., Depew, NY), WC (same as previously described), and ZrC (Catalogue No. ZR-303, 99.8% purity, <150 μm diameter, Atlantic Equipment Engineers, Bergenfield, NJ) powders. The W, WC, and ZrC powders were mixed in proportions consistent with the stoichiometry of reaction (1) for these calibration samples; that is, the powder mixtures ranged from 100 mol% WC (i.e., an "unreacted" standard powder composition) to 0 mol% WC (i.e., a "fully-reacted" 50 mol% W + 50 mol% ZrC standard powder composition). For each of

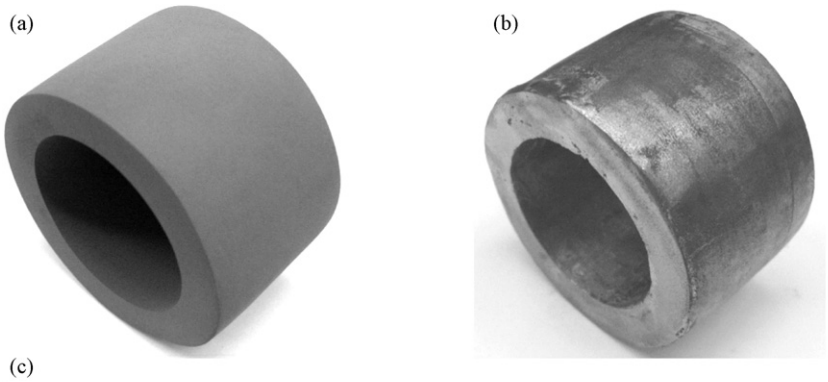

(c)

Specimen Description	Outer Diameter	Inner Diameter	Outer Height	Inner Height
Porous (53.3%) CNC-machined WC preform (before infiltration)	55.62 ± 0.07 mm	36.71 ± 0.08 mm	35.20 ± 0.07 mm	24.34 ± 0.06 mm
ZrC/W-bearing specimen (after reactive infiltration)	55.19 ± 0.05 mm	36.44 ± 0.09 mm	35.00 ± 0.06 mm	24.22 ± 0.05 mm
	$100\cdot\Delta D/D_o$ (ave.) = -0.77%	$100\cdot\Delta D/D_o$ (ave.) = -0.74%	$100\cdot\Delta L/L_o$ (ave.) = -0.57%	$100\cdot\Delta L/L_o$ (ave.) = -0.49%

Fig. 6. Optical photographs of a crucible-shaped sample at various stages of fabrication. (a) A porous, rigid, crucible-shaped WC preform prepared by uniaxial pressing of a WC/binder (ammonium acetate) mixture, binder removal and partial sintering (for necking of WC particles) at 1450 °C for 4 h, and then CNC machining. (b) A ZrC/W-bearing crucible-shaped specimen prepared by immersion of the CNC-machined, porous, crucible-shaped WC preform in (a) in the Zr_2Cu melt at 1150 °C for 30 min, then further reaction above the melt at 1300 °C for 2 h, and removal of residual adherent Cu-rich metal from the external surfaces. (c) Measured dimensions of the reactively-infiltrated specimen in (b), and of the associated porous preform in (a) prior to infiltration.

the "partially-reacted" standard powder mixtures, the total number of moles of WC + W was kept constant and the number of moles of ZrC and W were kept equal. The ratio of the area under the (1 1 0) W diffraction peak (centered at $2\theta = 40.3^\circ$) to the area under the (1 0 0) WC diffraction peak (centered at $2\theta = 35.6^\circ$) was plotted against the molar ratio of W:WC for each powder mixture to generate a XRD calibration curve. Nine samples of each powder mixture were evaluated with XRD analyses to obtain an average value (and the standard deviation) for the W:WC molar ratio. XRD analysis of a given cross-section of

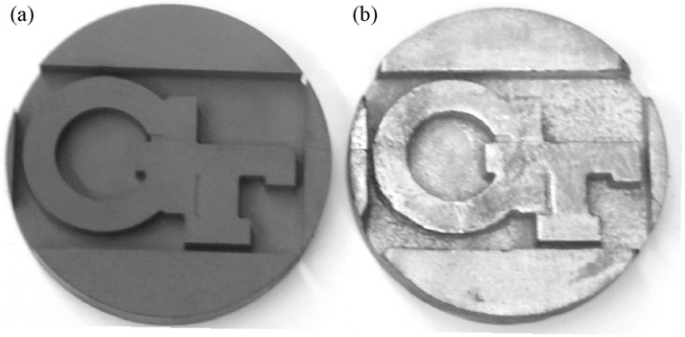

(c)

Specimen Description	Outer Disk Diameter	Disk Thickness	Outer Diameter of Letter "G"	Height of Letter "T"
Porous (49.8%) CNC-machined WC preform (before infiltration)	56.62 ± 0.06 mm	9.59 ± 0.20 mm	27.68 ± 0.10 mm	18.20 ± 0.11 mm
ZrC/W-bearing specimen (after reactive infiltration)	56.32 ± 0.12 mm	9.53 ± 0.18 mm	27.60 ± 0.12 mm	18.16 ± 0.09 mm
	$100\cdot\Delta D/D_o$ (ave.) = -0.53%	$100\cdot\Delta L/L_o$ (ave.) = -0.63%	$100\cdot\Delta D/D_o$ (ave.) = -0.29%	$100\cdot\Delta L/L_o$ (ave.) = -0.22%

Fig. 7. Optical photographs of two surface-machined disk samples at various stages of fabrication. (a) A porous, rigid WC preform prepared by uniaxial pressing of a WC/binder (ammonium acetate) mixture, binder removal and partial sintering (for necking of WC particles) at 1450 °C for 4 h, and then CNC machining. (b) ZrC/W-bearing specimen prepared by immersion of a CNC-machined, porous WC preform in the Zr_2Cu melt at 1150 °C for 30 min, then further reaction above the melt at 1300 °C for 2 h, and removal of residual adherent Cu-rich metal from the external surfaces. (c) Measured dimensions of the reactively-infiltrated specimen in (b), and of the associated porous preform prior to infiltration.

a reactively-infiltrated specimen was repeated 10 times to obtain an average W:WC ratio of integrated peak areas.

3. Results and discussion

3.1. Characterization of the Zr–Cu ingot and shaped porous WC preforms

XRD analysis of the solidified, arc-melted Zr–Cu ingot is shown in Fig. 2a. Diffraction peaks in this pattern were consistent with the congruently-melting Zr_2Cu compound ($T_m = 1000\,^{\circ}C$[43]), which indicated that the repeated arc melting and stirring process was effective for chemical homogenization. Representative XRD analyses obtained from cross-sections of WC preforms prepared by CNC machining or 3D printing (after binder burnout and partial sintering) are shown in Fig. 2b and c, respectively. The diffraction peaks in these XRD patterns were consistent with WC, which confirmed both the phase purity of the starting carbide powders and the absence of detectable solid tungsten oxides (WO_2, $W_{18}O_{49}$, $W_{20}O_{58}$, WO_3) as contaminant phases after the binder removal and partial sintering (WC necking) heat treatments. Optical images of porous, rigid WC preforms possessing nozzle, cone, crucible, and surface-patterned disk shapes prepared by CNC machining or by 3D printing are shown in Figs. 3a, 4a, 5a, 6a, and 7a. Values of the dimensions of such porous CNC-machined or 3D printed preforms are shown in Figs. 3d, 4d, 5c, 6c, and 7c.

3.2. Shape-preserving conversion of porous WC preforms into ZrC/W-based composites

Reactively-infiltrated specimens were generated by immersion of porous, rigid WC preforms in the Zr_2Cu melt at 1150 °C for 30 min, further reaction above the melt at 1300 °C for 2 h, and then cooling to room temperature. During and after pressureless infiltration, the Zr in the melt underwent selective reaction with the WC particles to yield a Cu-rich liquid that was then forced to external surfaces as the prior pores became filled with the solid ZrC and W products of reaction (1). The presence of residual, adherent copper-rich metal can be seen on the surfaces of the reactively-infiltrated nozzle specimens in Figs. 3b and 4b. Such solidified metal was easily removed from the reacted specimens by light polishing with SiC-bearing paper (note: the external copper-rich metal was much softer than the underlying carbide-bearing composite) to yield the specimens shown in Figs. 3c, 4c, 5b, 6b, and 7b. The shapes and dimensions of the starting preforms were well preserved in these reactively-infiltrated products. As revealed by the data in Figs. 3d, 4d, 5c, 6c, and 7c, measurements obtained at similar locations on the preform and reactively-infiltrated specimens yielded average dimensional changes consistently under 1% (*note*: the average values shown in these figures were obtained from at least five measurements of a given specimen dimension and the indicated variance values refer to the entire range of measured values). Indeed, even surface features were preserved upon reactive infiltration. For example, slight surface indentations made by the milling bit used to machine the porous

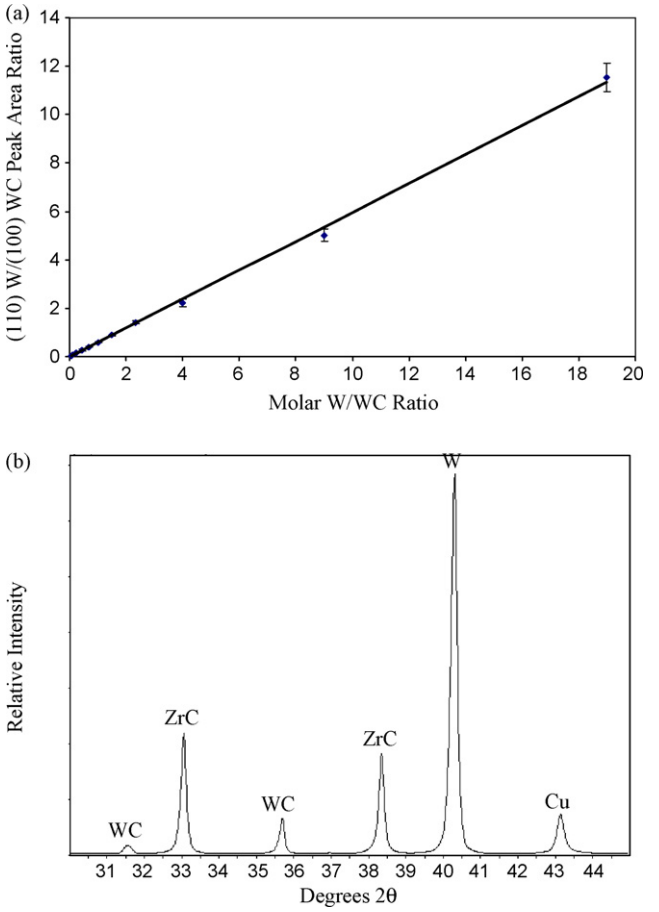

Fig. 8. (a) XRD calibration curve for evaluating the W:WC molar ratio in partially-reacted specimens. (b) XRD analysis of a cross-section of a composite specimen generated by the reactive infiltration of a 57.7% porous, 3D printed, disk-shaped WC preform with molten Zr_2Cu (at 1150 °C for 30 min, then 1300 °C for 2 h).

WC nozzle preforms (such as in Fig. 3a) can be seen in the reactively-infiltrated ZrC/W-bearing nozzle in Fig. 3c.

3.3. Microstructural analyses of DCP-converted ZrC/W-based composites

Reactively-infiltrated specimens were cross-sectioned and polished for electron microscopy and quantitative XRD analyses. These specimens were generated from disk-shaped WC preforms with porosity values of 52.3% and 53.7% (prepared by pressing WC/rice starch and WC/ammonium acetate mixtures, respectively, and thermal treatment at a peak temperature of 1450 °C for 4 h) and 57.7% (prepared by 3D printing and thermal treatment at a peak temperature of 2100 °C for 4 h). The calibration curve used for quantitative XRD phase analyses is shown in Fig. 8a. A representative XRD pattern obtained from the reactively-infiltrated, 3D printed specimen (with a starting preform porosity of 57.7%) is shown in Fig. 8b. Diffraction peaks for the ZrC and W products of reaction (1), along with some unreacted WC and retained Cu, were detected. Diffraction peaks for W_2C or zirconium-depleted Zr–Cu compounds (e.g., Zr_7Cu_{10}, Zr_3Cu_8, $Zr_{14}Cu_{51}$, Zr_2Cu_9[43]) were not observed. The absence

Table 1
Characteristics of ZrC/W-bearing composites.

WC preform forming method; max. thermal treatment; rel. porosity	W:WC molar ratio	$\Delta W/W_o$[a] (%)	ρ[exptl.] (g/cm^3)	Phase content[b] (vol.%)				ρ[theo.][c] (g/cm^3)
				ZrC	W	WC	Cu	
Pressing WC/rice starch; 1450 °C, 4 h; 52.3 ± 0.1%	11.5 ± 0.8	48.7 ± 0.1	10.99 ± 0.05	56 ± 6	35 ± 4	3.9 ± 0.4	5.1 ± 0.6	11.5 ± 0.9
Pressing WC/NH_4 acetate; 1450 °C, 4 h; 53.7 ± 0.1%	8.7 ± 0.6	52.5 ± 0.1	11.61 ± 0.05	53 ± 6	33 ± 4	4.9 ± 0.5	9 ± 1	11.4 ± 1.2
3D printing; 2100 °C, 4 h; 57.7 ± 0.1%	21 ± 2	56.6 ± 0.1	10.58 ± 0.05	55 ± 6	33 ± 4	2.1 ± 0.2	10 ± 1	11.2 ± 1.2

[a] $\Delta W/W_o = 100 \times$ [weight change upon reactive infiltration]/[weight of starting porous WC preform]. The variance ranges for $\Delta W/W_o$ (and for ρ[exptl.]) refer to the error due to the precision of the balance.
[b] Phase content after reactive infiltration, derived from the W:WC molar ratio and $\Delta W/W_o$.
[c] ρ[theo.] = theoretical density values for the ZrC–W–WC–Cu mixtures shown in the column to the left.

of the latter Zr–Cu compounds was consistent with essentially complete consumption of zirconium from the infiltrated Zr_2Cu melt by reaction with WC (note: the maximum solid solubility of zirconium in copper is reported to be only 0.12 at.%[43]). XRD patterns obtained from the reactively-infiltrated pressed specimens (with starting preform porosity values of 52.3% and 53.7%) exhibited diffraction peaks located at similar 2θ positions (i.e., the only phases detected in each of these specimens

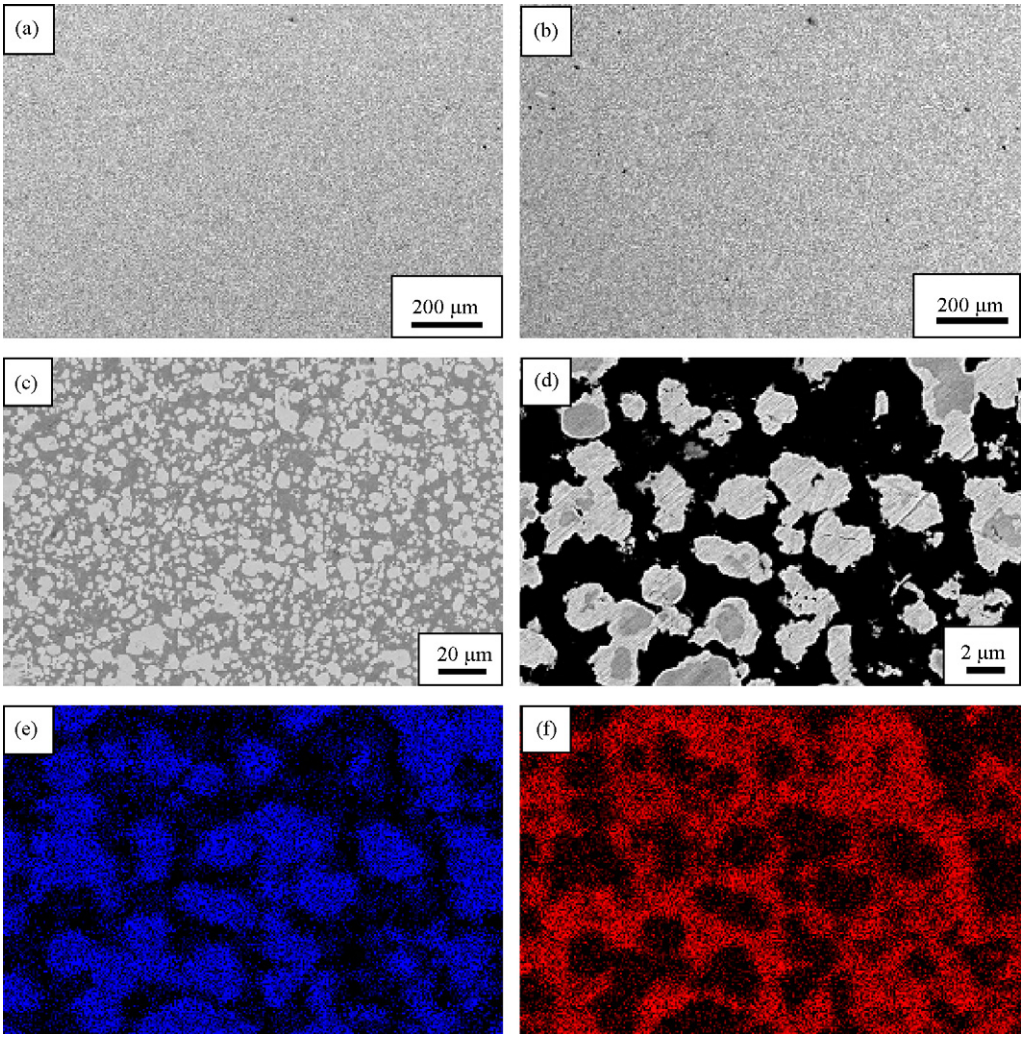

Fig. 9. Electron microscope images obtained from polished cross-sections of a ZrC/W-bearing specimen prepared by reactive infiltration of a 52.3% porous WC preform with molten Zr_2Cu at 1150 °C for 30 min, then at 1300 °C for 2 h. The WC preform was generated from a pressed WC/starch mixture heated to a peak temperature of 1450 °C for 4 h. Corresponding low-magnification secondary electron and backscattered electron images are shown in (a) and (b). Higher magnification backscattered electron images are shown in (c) and (d). X-ray maps for W and Zr, corresponding to the backscattered electron image in (d), are shown in (e) and (f), respectively.

were ZrC, W, WC, and Cu). For each specimen, the ratio of the area under the (1 1 0) W diffraction peak (centered at $2\theta = 40.3^\circ$) to the area under the (1 0 0) WC diffraction peak (centered at $2\theta = 35.6^\circ$) was evaluated. The calibration curve in Fig. 8a was then used to obtain a molar W:WC ratio for each specimen, and these values are listed in Table 1.

Electron micrographs of a polished cross-section of a ZrC/W-bearing composite specimen generated by the reactive infiltration of the 52.3% porous preform (formed by pressing and thermal treatment of a WC/rice starch mixture) are shown in Fig. 9. The low- and intermediate-magnification secondary and backscattered electron images in Fig. 9a–d reveal a dense composite with very few isolated (dark) pores. The intermediate- and high-magnification backscattered electron images in Fig. 9c and d show that the composite was comprised of a particulate material distributed uniformly within a darker (lower atomic number) matrix. The higher magnification backscattered electron image in Fig. 9d indicated that the particles were comprised of either: (i) a darker core and a brighter (higher atomic number) cladding phase, or (ii) just the relatively bright phase. The tungsten X-ray map in Fig. 9e indicated that both the darker particle cores within some particles and the bright phase contained tungsten. The zirconium X-ray map in Fig. 9f indicated that the particles and matrix phase were depleted and enriched, respectively, in zirconium. Energy dispersive X-ray (EDX) analyses of the darker cores of some of these particles (such as shown in Fig. 10a) yielded distinct peaks for tungsten and carbon, which was consistent with the unreacted tungsten carbide detected by XRD analyses. EDX analyses of the dark matrix phase (Fig. 10c) indicated an enrichment of zirconium and carbon, which was consistent with the zirconium carbide product of reaction (1). EDX analyses of the bright phase surrounding some of the particles, and comprising the entirety of the other particles, yielded less carbon relative to tungsten (compare the EDX patterns in Fig. 10a and b), which was consistent with the tungsten product of reaction (1) (*note*: much of the C detected in Fig. 10b was likely a result of overlap of some of the beam interaction volume with the surrounding ZrC matrix phase and/or adjacent underlying WC). A modest amount of copper was also occasionally detected by EDX analysis of relatively large areas (550 μm × 360 μm, Fig. 10d). Hence, the electron microscope/EDX and XRD analyses indicated that this specimen was comprised of a uniform distribution of W-coated WC particles and fully-converted W particles within a matrix of ZrC with some residual Cu. Similar microstructures were observed for the composite specimen generated by reactive infiltration of a pressed/partially sintered 53.7% porous preform (formed by pressing a WC/ammonium acetate mixture, binder burnout, and thermal treatment at 1450 °C for 4 h).

Electron micrographs of a polished cross-section of a ZrC/W-bearing composite specimen generated by the reactive infiltration of a 57.7% porous, 3D printed preform (after binder

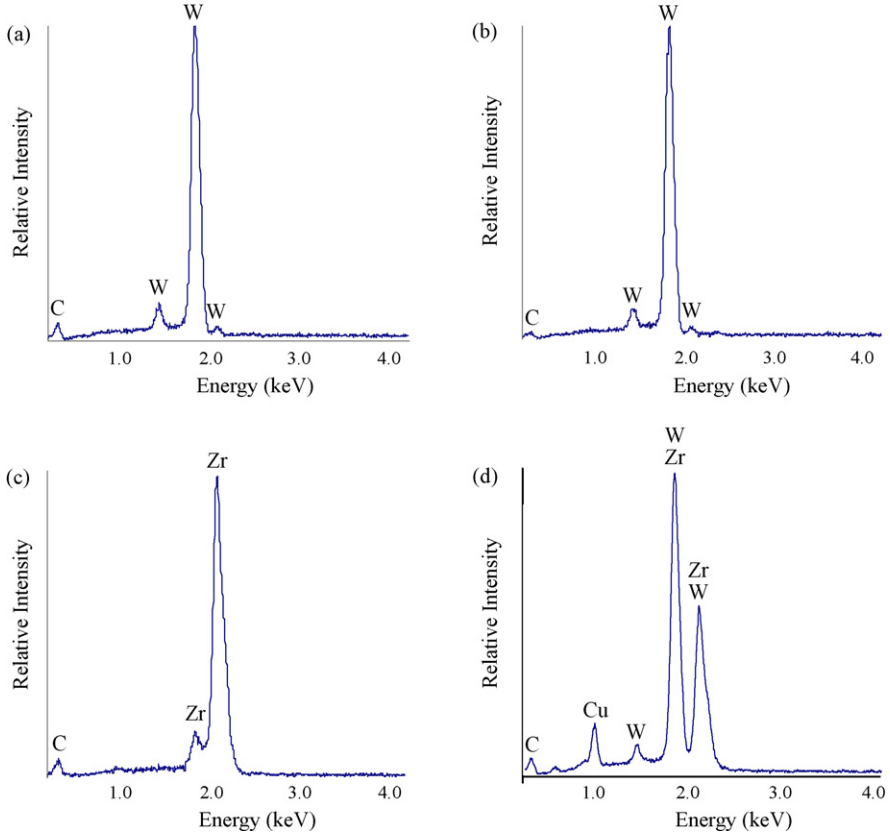

Fig. 10. Representative energy dispersive X-ray (EDX) analyses obtained from phases seen in Fig. 9(d). These EDX patterns were obtained from: (a) the grey (WC) core present within some of the particles, (b) the bright (W) cladding coating partially-reacted particles, and (c) the dark (ZrC) matrix region. (d) EDX analysis of a 550 μm × 360 μm area of a polished cross-section of this specimen revealing a modest Cu peak.

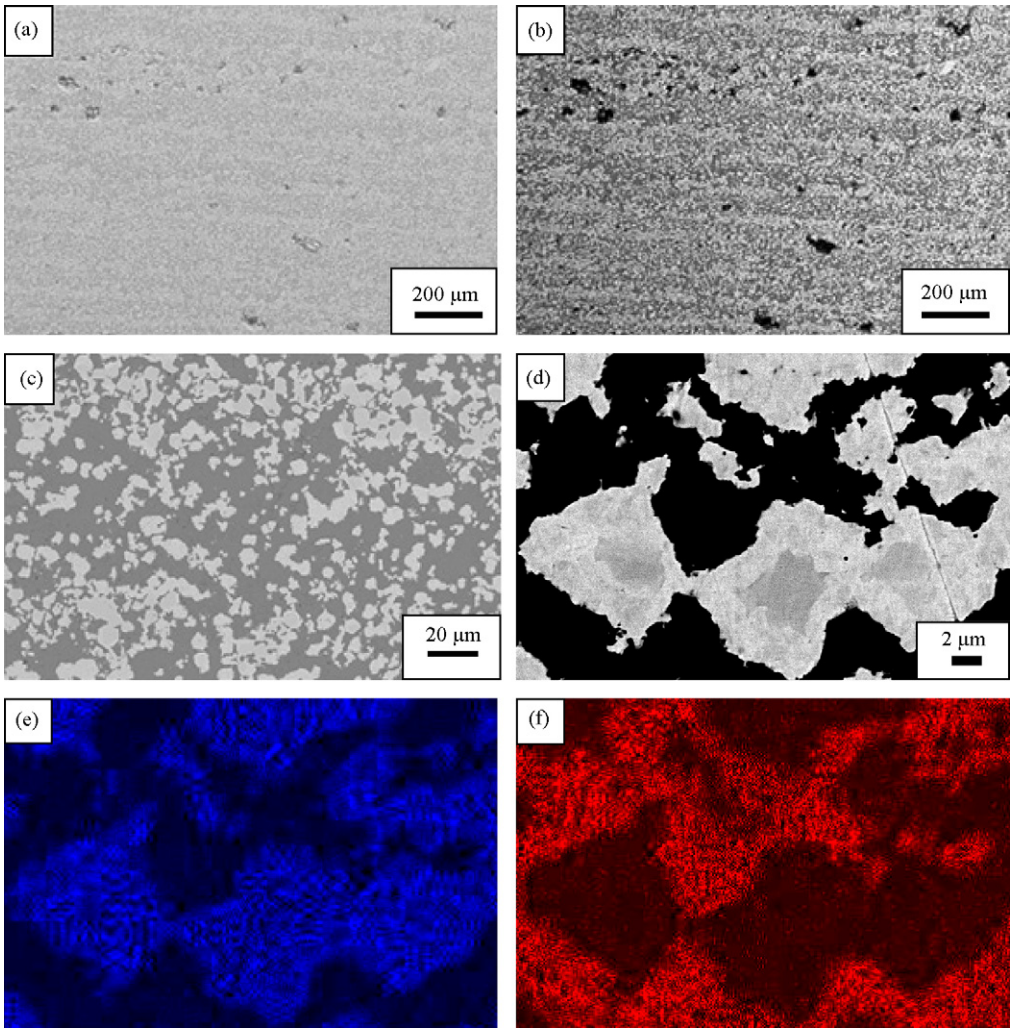

Fig. 11. Electron microscope images obtained from polished cross-sections of a ZrC/W-bearing specimen prepared by reactive infiltration of a 57.7% porous WC preform with molten Zr_2Cu at 1150 °C for 30 min, then at 1300 °C for 2 h. The WC preform was generated from a 3D printed WC preform fired at a peak temperature of 2100 °C for 4 h. Corresponding low-magnification secondary electron and backscattered electron images are shown in (a) and (b). Higher magnification backscattered electron images are shown in (c) and (d). X-ray maps for W and Zr, corresponding to the backscattered electron image in (d), are shown in (e) and (f), respectively.

removal and then thermal treatment at a peak temperature of 2100 °C for 4 h) are shown in Fig. 11. The low- and intermediate-magnification secondary and backscattered electron images in Fig. 11a–d reveal a relatively dense composite containing isolated (dark) pores. However, more pores were detected within this specimen than within the specimen shown in Fig. 9. The low-magnification images in Fig. 11a and b also indicated that this composite (unlike the composite in Fig. 9) was comprised of alternating layers enriched in the bright particles or the darker matrix phase. The thickness of each pair of particle-rich and matrix-rich layers was ~120 μm, which was similar to the thickness of each WC layer deposited in the 3D printing process; that is, such a layered composite microstructure was apparently inherited from the layer-by-layer 3D printing of WC particles. The higher magnification backscattered electron image in Fig. 11d revealed particles that were comprised of either a single bright phase or of a darker core with a bright cladding. The tungsten and zirconium X-ray maps in Fig. 11e and f indicated that the particles and the matrix phase were enriched in tungsten and zirconium, respectively. EDX analyses of these phases indicated, as for the composite in Fig. 9, that the particles were comprised of W or W-coated WC and the darker matrix was comprised of ZrC with a small amount of residual Cu.

3.4. Quantitative phase analyses of DCP-converted ZrC/W-based composites

The partial conversion of a porous WC preform into a composite comprised of a mixture of ZrC(s) and W(s), along with residual WC(s) and Cu(s), may be described by the following reaction (written on the basis of 1 mole of WC reactant):

$$(a/2)Zr_2Cu(l) + WC(s) \rightarrow aZrC(s) + aW(s) + (1-a)WC(s) + bCu(s) + [(a/2)-b]\{Cu\} \quad (2)$$

where {Cu} refers to molten copper ($T_m = 1085$ °C[43]) that has been extruded out of the reacted specimen at 1150–1300 °C due to the filling of prior pores with solid products (W + ZrC) that

possessed a larger volume than the starting WC. The values of the parameters a and b in reaction (2) for a given composite specimen may be evaluated from the W:WC molar ratio (obtained from quantitative XRD analysis) and the weight change upon reactive infiltration, $\Delta W/W_o$. Such data is presented in Table 1 for the reactively-infiltrated, disk-shaped specimens discussed in Section 3.3. Consider, for example, the reactively-infiltrated specimen generated from the 52.3% porous WC preform (prepared from a pressed and thermally treated WC/rice starch mixture). Quantitative XRD analysis indicated that this composite possessed a molar W:WC ratio of 11.5. The corresponding value of a in reaction (2) for this specimen was 0.92. The weight gain upon reactive infiltration of this preform was 48.7%. This weight gain was used, along with the known values of molar volume (V_m)[11] and molecular/atomic weight (MW/AW) for ZrC, WC, W, and Cu, to calculate the value of b, as shown by the following equation:

$$\frac{\Delta W}{W_o} = 0.487 = \frac{\{[a \cdot MW_{ZrC} + a \cdot AW_W + (1-a) \cdot MW_{WC} + b \cdot AW_{Cu}] - MW_{WC}\}}{[MW_{WC}]}$$

$$= \frac{\{[0.920\,\text{mol} \cdot 103.23\,\text{g/mol} + 0.920\,\text{mol} \cdot 183.85\,\text{g/mol} + 0.080\,\text{mol} \cdot 195.86\,\text{g/mol} + b \cdot 63.55\,\text{g/mol}] - 195.86\}}{195.86}$$

Use of this equation yielded a value of 0.180 mole for b. The values of a and b obtained for this reacted specimen corresponded to a mixture of 56 vol% ZrC, 35 vol% W, 3.9 vol% WC, and 5.1 vol% Cu. Similar calculations for reactively-infiltrated specimens generated from 53.7% to 57.2% porous WC preforms (prepared from a pressed/partially sintered WC/ammonium acetate mixture and a 3D printed/partially sintered WC preform, respectively) yielded the composite phase contents shown in Table 1. The phase contents for all three of these composite specimens fell in the range: 55 ± 2 vol% ZrC, 34 ± 1 vol% W, 3.6 ± 1.5 vol% WC, 7.5 ± 2.5 vol% Cu. The theoretical densities of these ZrC–W–WC–Cu phase mixtures are shown in the rightmost column of Table 1. Comparison of these theoretical density values to the measured bulk density values indicated that the composites generated from the pressed preforms possessed relative densities of 95–100%, whereas the composite generated from the 3D printed preform possessed a relative density of 94%. The lower calculated relative density of the latter specimen was consistent with the detection of additional pores within polished cross-sections of this specimen (Fig. 11a and b), and was likely a result of the higher starting porosity, and perhaps the less uniform pore size distribution, of the 3D printed WC preform relative to the pressed WC preforms.

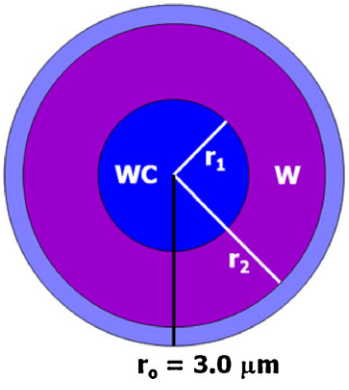

Percent Conversion	r_1 (μm)	r_2 (μm)	r_1/r_2
90	1.39	2.77	0.50
95	1.11	2.76	0.40
99	0.65	2.74	0.24
99.9	0.30	2.74	0.11

Fig. 12. Schematic illustration of the partial conversion of a spherical WC particle into W via reaction (1). r_0, r_1, and r_2 refer to the radii of the starting WC sphere (before reaction), the radius of the unreacted WC core, and the total radius (W + WC) of a partially-reacted sphere, respectively. Percent conversion refers to the extent of conversion (in mol%) of the original WC sphere into W. (*Note*: the ZrC product that surrounds the W product is not shown here.)

At first glance, the amount of residual, unreacted WC relative to the W product seen in the electron micrographs of Figs. 9 and 11 may appear larger than expected for the ratio of WC to W determined for the composite mixtures shown in Table 1. However, this illusory discrepancy is the result of the relatively large volume occupied by the W product layer surrounding the WC core of an incompletely-reacted WC particle. Consider, for simplicity, a spherical WC particle with a diameter of 6 μm, as illustrated in Fig. 12. If 90.0 mol% of the WC in this spherical particle is converted into W, so as to yield a W-coated WC particle with a WC:W volume ratio of 0.146:1, then the resulting particle would possess a WC core with a diameter of 2.79 μm surrounded by a 1.38 μm thick W layer (i.e., the diameter of the unreacted WC core would comprise 50.3% of the total W/WC particle diameter). For 99.0 mol% WC conversion (to yield a W-coated WC particle with a WC:W volume ratio of 0.013:1), the resulting particle would contain a 1.30 μm diameter WC core surrounded by a 2.09 μm thick W layer (i.e., the WC core diameter would comprised 23.7% of the total W/WC particle diameter). Hence, the presence of some partially-reacted particles with relatively large unreacted cores in Figs. 9 and 11 was not inconsistent with the data shown in Table 1.

4. Conclusions

Two automated rapid prototyping processes have been evaluated for fabricating complex-shaped porous WC preforms for subsequent reactive infiltration via the Displacive Compensation of Porosity (DCP) process: (i) computer-numerical-controlled (CNC) machining of compacted and partially sintered (porous, rigid) WC cylinders, and (ii) three-dimensional (3D) printing of WC powder. Mixtures of WC powder with an ammonium acetate or rice starch binder were uniaxially pressed, exposed to a binder removal treatment, and then thermally treated at a peak temperature of 1450 °C to yield rigid, cylindrical preforms with 51.7 ± 2.0% porosity. These WC preforms were then green machined into rocket nozzle, cone, crucible, and surface-patterned disk shapes with a CNC milling machine using a WC/Co milling bit. Porous WC preforms were also fabricated via layer-by-layer 3D printing of WC powder with a polyethyleneimine-based binder. After binder removal and thermal treatment at a peak temperature of 2100 °C for 4 h, rigid, nozzle- and disk-shaped WC preforms with porosity values of 57.9 ± 0.2% were obtained. Molten Zr_2Cu was allowed to infiltrate at ambient pressure into the

porous CNC-machined and 3D printed preforms during immersion for 30 min at 1150 °C. The infiltrated specimens were then raised above the melt and heated to 1300 °C for 2 h to allow for further reaction. Weight change measurements and quantitative X-ray diffraction analyses indicated that reactively-infiltrated specimens derived from pressed/CNC-machined and 3D printed preforms were comprised of 55 ± 2 vol% ZrC and 34 ± 1 vol% W, along with 3.6 ± 1.5 vol% unreacted WC and 7.5 ± 2.5 vol% retained Cu, and possessed relative densities of 95–100% and 94%, respectively. Electron microscopic analyses indicated that the DCP-derived, ZrC/W-based composites generated from 3D printed preforms were dense (i.e., with closed, isolated porosity) and possessed a layered morphology (with alternating ZrC-rich and W-rich layers), whereas dense DCP-derived composites formed from pressed/CNC-machined preforms possessed a relatively uniform distribution of ZrC and W phases. DCP-converted, ZrC/W-based nozzle-, cone-, crucible-, and surface-patterned disk specimens generated from both pressed/CNC-machined and 3D printed preforms retained the preform shapes and dimensions to within 1%. This work demonstrates, for the first time, that the flexible shape-forming ability of CNC green machining or 3D printing may be coupled with the shape/dimension-preserving capability of the DCP process to allow for the rapid fabrication of dense, ultrahigh-melting carbide/refractory metal composites with readily-tailored, near net-shapes and dimensions.

Acknowledgements

This research was supported by the Air Force Office of Scientific Research (Award No. FA9550-07-1-0115, Dr. Joan Fuller, Program Manager).

References

1. *Solid Rocket Motor Nozzles*, NASA Special Publ. SP-8115, June 1975.
2. Sutton GP. *Rocket propulsion elements*. New York, NY: John Wiley & Sons; 1992. p. 483–488.
3. Upadhya K, Yang J-M, Hoffman WP. Materials for ultrahigh temperature structural applications. *Bull Am Ceram Soc* 1997;**76**(12):51–6.
4. De Morton ME. Erosion in rocket motor nozzles. *Wear* 1977;**41**:223–31.
5. Vicario AA, Freeman WT, Casseday ED. High-temperature properties and failure criteria for rocket nozzle materials. *J Spacecraft* 1974;**11**:631–6.
6. Neilson JH, Gilchrist A. An experimental investigation into aspects of erosion in rocket motor tail nozzles. *Wear* 1968;**11**:123–43.
7. Olcott EL, Batchelor JD. Failure mechanisms in dense tungsten alloy rocket nozzles. *J Spacecraft* 1964;**1**:635–42.
8. Walton JD, Mason CR. Materials problems associated with uncooled rocket nozzles. *Corrosion* 1960;**16**:371t–4t.
9. Storms EK. *The refractory carbides*. New York, NY: Academic Press; 1967. p. 18–35.
10. Rudy E, Harmon DP, Brukl CE. In: McHale AE, editor. *Phase equilibria diagrams. Phase diagrams for ceramists*, vol. X. The American Ceramic Society; 1994 [Fig. 8963].
11. *JCPDS International Center for Diffraction Data File 00-035-0784 for ZrC, 00-025-1047 for WC, 00-004-0806 for W*. Newtown Square, PA: JCPDS International Center for Diffraction Data; 2007.
12. Nagender Naidu SV, Rama Rao P. In: Nagender Naidu SV, Rama Rao P, editors. *Phase diagrams of binary tungsten alloys*. Calcutta, India: Indian Institute of Metals; 1991. p. 1–3.
13. Gumbsch P, Riedle J, Hartmaier A, Fischmeister HF. Controlling factors for the brittle-to-ductile transition in tungsten single crystals. *Science* 1998;**282**:1293–5.
14. Dawson CW, Sell HG. *Metals handbook*, 3, 9th ed. American Society for Metals; 1980. p. 325–329.
15. Lassner E, Schubert W-D. *Tungsten—properties, chemistry, technology of the element, alloys and chemical compounds*. Springer-Verlag; 1999.
16. Song GM, Wang YJ, Zhou Y. The mechanical and thermophysical properties of ZrC/W composites at elevated temperatures. *Mater Sci Eng A* 2002;**A334**:223–32.
17. Eremenko VN, Velikanova TY, Artyukh LV, Aksel'rod GM, Vishnevskii AS. In: McHale AE, editor. *Phase equilibria diagrams. Phase diagrams for ceramists*, vol. X. The American Ceramic Society; 1994 [Fig. 9034].
18. Barin I. *Thermochemical data of pure substances*, vol. II, 3rd ed. Weinheim, Germany: VCH Verlagsgesellschaft; 1995. p. 1782–1783.
19. Touloukian YS, Kirby RK, Taylor RE, Desai PD. *Thermophysical properties of matter, vol. 12. Thermal expansion of metallic elements and alloys*. New York: Plenum Press; 1975. p. 354.
20. Touloukian YS, Kirby RK, Taylor RE, Lee TYR. *Thermophysical properties of matter, vol. 13. Thermal expansion of nonmetallic solids*. New York: Plenum Press; 1977. p. 926.
21. Touloukian YS, Powell RW, Ho CY, Klemens PG. *Thermophysical properties of matter, vol. 1. Thermal conductivity of metallic elements and alloys*. New York: Plenum Press; 1970. p. 428.
22. Touloukian YS, Powell RW, Ho CY, Klemens PG. *Thermophysical properties of matter, vol. 2. Thermal conductivity of nonmetallic solid*. New York: Plenum Press; 1970. p. 611.
23. Song GM, Wang YJ, Zhou Y. Elevated temperature ablation resistance and thermophysical properties of tungsten matrix composites reinforced with ZrC particles. *J Mater Sci* 2001;**36**:4625–31.
24. Zhang SC, Hilmas GE, Fahrenholtz WG. Zirconium carbide–tungsten cermets prepared by *in situ* reaction sintering. *J Am Ceram Soc* 2007;**90**:1930–3.
25. Dickerson MB, Wurm PJ, Schorr JR, Hoffman WP, Hunt E, Sandhage KH. Near net-shaped, ultra-high melting, recession-resistant ZrC/W-based rocket nozzle liners via the displacive compensation of porosity (DCP) method. *J Mater Sci* 2004;**39**:6005–15.
26. Dickerson MB, Snyder RL, Sandhage KH. Dense, near net-shaped, carbide/refractory metal composites at modest temperatures by the displacive compensation of porosity (DCP) method. *J Am Ceram Soc* 2002;**85**: 730–2.
27. Sandhage KH, Kumar P, Method for fabricating shaped monolithic ceramics and ceramic composites through displacive compensation of porosity, and ceramics and composites made thereby. *U.S. Patent No.* 6,833,337; December 21, 2004.
28. Sandhage KH, Unocic RR, Dickerson MB, Timberlake M, Guerra K, Method for fabricating high-melting, wear-resistant ceramics and ceramic composites at low temperatures. *U.S. Patent No.* 6,596,698; July 29, 2003.
29. Sandhage KH, Kumar P, Method for fabricating shaped monolithic ceramics and ceramic composites through displacive compensation of porosity, and ceramics and composites made thereby. *U.S. Patent No.* 6,407,022; June 18, 2002.
30. Kumar P, Sandhage KH. The displacive compensation of porosity (DCP) method for fabricating dense, shaped, high-ceramic-bearing bodies at modest temperatures. *J Mater Sci* 1999;**34**:5757–69.
31. Rogers KA, Kumar P, Citak R, Sandhage KH. The fabrication of dense, shaped ceramic/metal composites at $\leq$1000 °C by the displacive compensation of porosity method. *J Am Ceram Soc* 1999;**82**:757–60.
32. Rogers KA, Kumar P, Citak R, Sandhage KH. The displacive compensation of porosity (DCP) method for fabricating dense oxide/metal composites at modest temperatures with small dimensional changes. In: Bansal NP, Singh JP, editors. *Innovative processing and synthesis of ceramics, glasses, and composites II, Ceram. Trans., vol. 94*. 1999. p. 141–52.
33. Subramanian PR, Laughlin DE. In: Nagender Naidu SV, Rama Rao P, editors. *Phase diagrams of binary tungsten alloys*. Calcutta, India: Indian Institute of Metals; 1991. p. 76–9.
34. Dickerson MB, Snyder RL, Sandhage KH. Low-temperature fabrication of dense, near net-shaped tungsten/zirconium carbide composites with tai-

lored phase contents by the PRIMA-DCP process. *Ceram Eng Sci Proc* 2001;**22**:97–107.

35. Dickerson MB, Sandhage KH. Low-temperature reaction casting of dense, near net-shaped carbide/refractory metal composites with tailored phase contents. *Latin Am J Metall Mater* 2001;**21**:18–24.
37. Dickerson MB, Unocic RR, Guerra KT, Timberlake MJ, Sandhage KH. The fabrication of dense carbide/refractory metal composites of near net shape at modest temperatures by the PRIMA-DCP process. In: Bansal NP, Singh JP, editors. *Innovative processing and synthesis of ceramics, glasses, and composites IV, Ceram. Trans., vol. 115*. 2000. p. 25–31.
38. Moon J, Caballero AC, Hozer L, Chiang Y-M, Cima MJ. Fabrication of functionally graded reaction infiltrated SiC–Si composite by three-dimensional printing (3DP^{TM}) process. *Mater Sci Eng A* 2001;**A298**:110–9.
39. Atisivan R, Bandyopadhyay A, Gupta YM. Dynamic tensile response of alumina–Al composites. In: *Shock compression of condensed matter, AIP conf. proc*. 2002. p. 697–700.
40. Yin X, Travitzky N, Melcher R, Greil P. Three-dimensional printing of $TiAl_3/Al_2O_3$ composites. *Int J Mater Res* 2006;**97**:492–8.
41. Yin X, Travitzky N, Greil P. Three-dimensional printing of nanolaminated Ti_3AlC_2 toughened $TiAl_3/Al_2O_3$ composites. *Int J Mater Res* 2006;**97**:492–8.
42. Zhang W, Travitzky N, Greil P. Formation of $NbAl_3/Al_2O_3$ composites by pressureless reactive infiltration. *J Am Ceram Soc* 2008;**91**: 3117–20.
43. Arias D, Abriata JP. Cu–Zr (copper–zirconium). *Bull Alloy Phase Diagr* 1990;**11**:452–9.